Electronic Supplementary Material (ESI) for Dalton Transactions.
This journal is © The Royal Society of Chemistry 2022

Electronic Supplementary Information

Rational synthesis of a pyridyl-imidazoquinazoline based multifunctional 3D Zn(II)-MOF: structure, luminescence, selective and sensitive detection of Al^{3+} and TNP, and its semiconducting device application

Gurupada Bairy,[†,#] Arka Dey,[£,#] Basudeb Dutta,[§] Suvendu Maity,[†] Chittaranjan Sinha*[,†]

[†]Department of Chemistry, Jadavpur University, Kolkata 700 032, India. Mail id: crsjuchem@gmail.com

[£]Department of Physics, National Institute of Technology Durgapur, Durgapur 713209, India.

[§]Department of Chemical Sciences, Indian Institute of Science Education and Research Kolkata, Mohanpur 741246 West Bengal, India.

[#]Both the authors contributed equally to this work.

Sl. No.	Contents	Page No.
1.	Schematic representation of the synthesis of 6-(pyridin-4-yl)-5,6-dihydrobenzo[4,5]imidazo[1,2-c]quinazoline (pdiq).	**4**
2.	Schematic representation of the synthesis of **1**.	**4**
3.	Mass spectrum of pdiq.	**4**
4.	^{1}H and ^{13}C spectroscopy of pdiq.	**5**
5.	IR spectroscopy of pdiq and **1**.	**6**
6.	Crystallographic data of **1** (**Table S1**).	**7**
7.	Bond lengths and bond angles in **1** (**Table S2**).	**8**
8.	Powder X-ray Diffraction analysis of **1**.	**9**
9.	Thermogravimetric analysis (TGA) of **1**.	**9**
10.	UV Visible spectrum of **1**.	**10**
11.	Absorption spectra of **1** in presence of different metal ions.	**10**
12.	Emission spectra of **1** in presence of different metal ions.	**11**
13.	Stern-Volmer plot of **1** at lower concentrations of Al(III).	**11**
14.	Limit of detection plot and calculation of detection limit of **1** for Al(III).	**12**
15.	^{1}H-NMR titration between **1** and Al^{3+} in d^{6}-DMSO medium.	**13**
16.	Life time plot of **1** in the absence and presence of Al(III).	**13**
17.	Lifetime decay parameters of **1** for Al(III) (**Table S3**).	**14**
18.	Emission spectra of **1** in presence of different NAEs.	**14**

19.	Stern-Volmer plot of **1** for TNP.	**15**
20.	Limit of detection (LOD) plot of **1** for TNP.	**15**
21.	Calculation of detection limit of **1** for TNP.	**16**
22.	Life time plot of **1** for TNP.	**16**
23.	Lifetime decay parameters of **1** for TNP (**Table S4**).	**17**
24.	HOMO and LUMO energies for **1** (**Table S5**).	**17**
25.	Emission spectra of **1** in presence of different PH solutions.	**18**
26.	Overlapping of absorption spectra of TNP with emission spectra of **1**.	**18**
27.	1D ribbon like network from a portion of molecular assembly.	**19**
28.	The ORTEP diagram of **1** showing disorder of 2,5-tda ligand.	**19**
29.	Paper strip experiment for recyclability of **1** towards Al^{3+} sensing.	**20**
30.	Optical Characterization.	**20**
31.	Device Fabrication.	**21**
32	Electrical Property Analysis.	**21-23**
33	References.	**23-25**

Scheme S1. Synthesis of 6-(pyridin-4-yl)-5,6-dihydrobenzo[4,5]imidazo[1,2-c]quinazoline (pdiq).

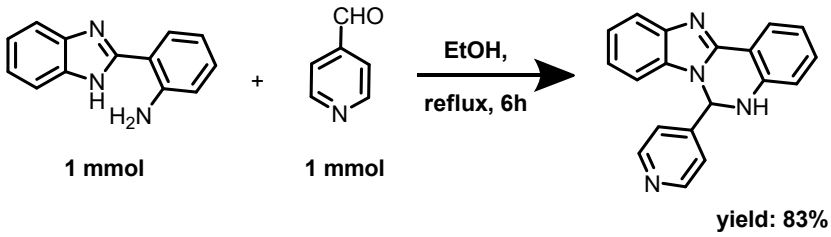

Scheme S2. Synthesis of $[Zn_2(tdc)_4(pdiq)_3)]$ (**1**).

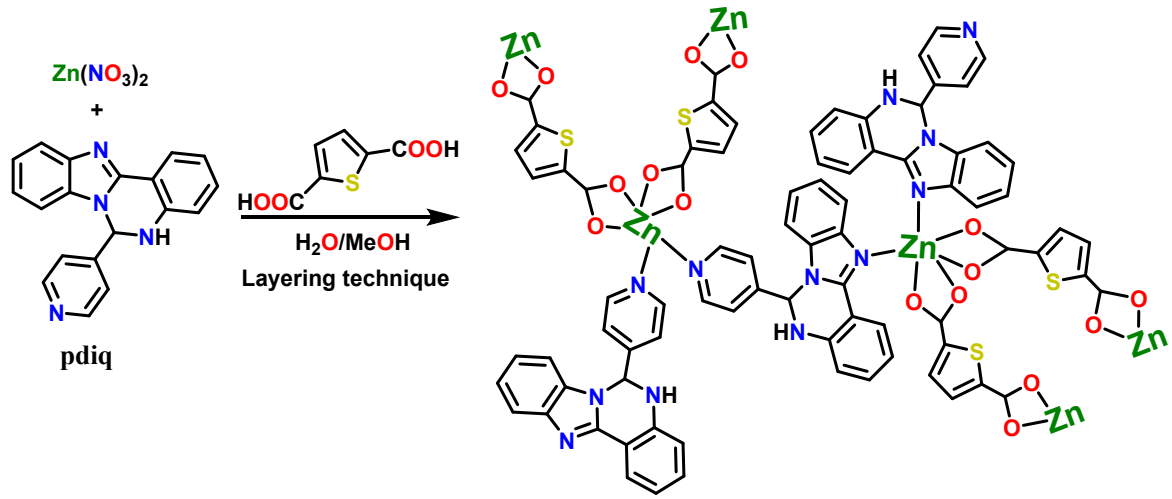

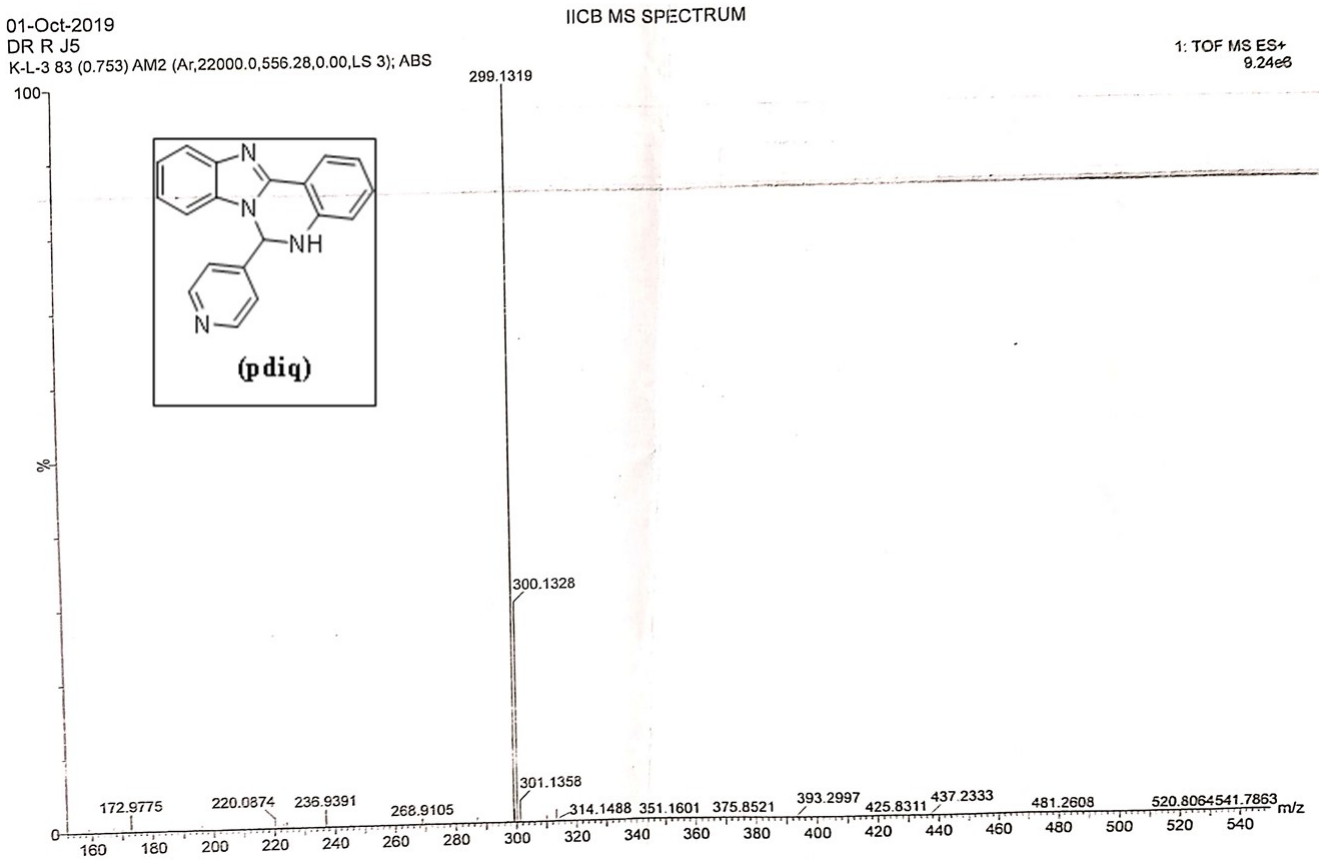

Fig. S1 Mass spectrum of **pdiq**.

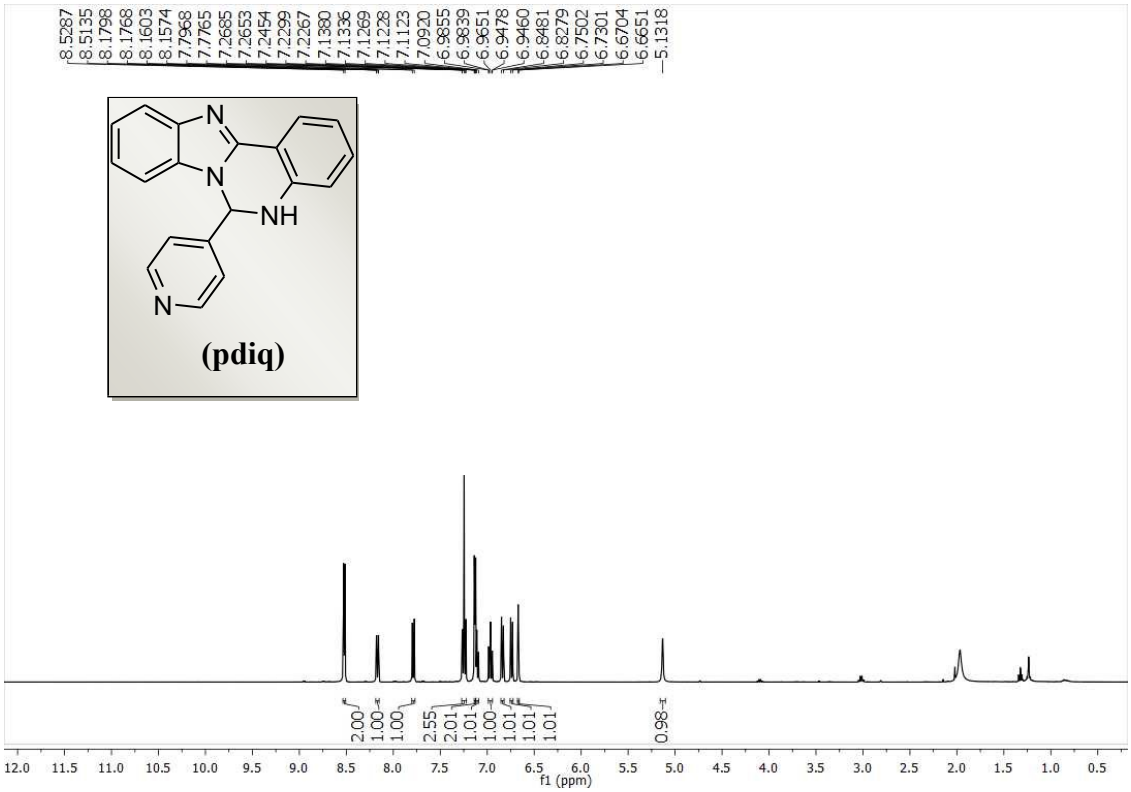

Fig. S2 ^{1}H-NMR spectrum of **pdiq**.

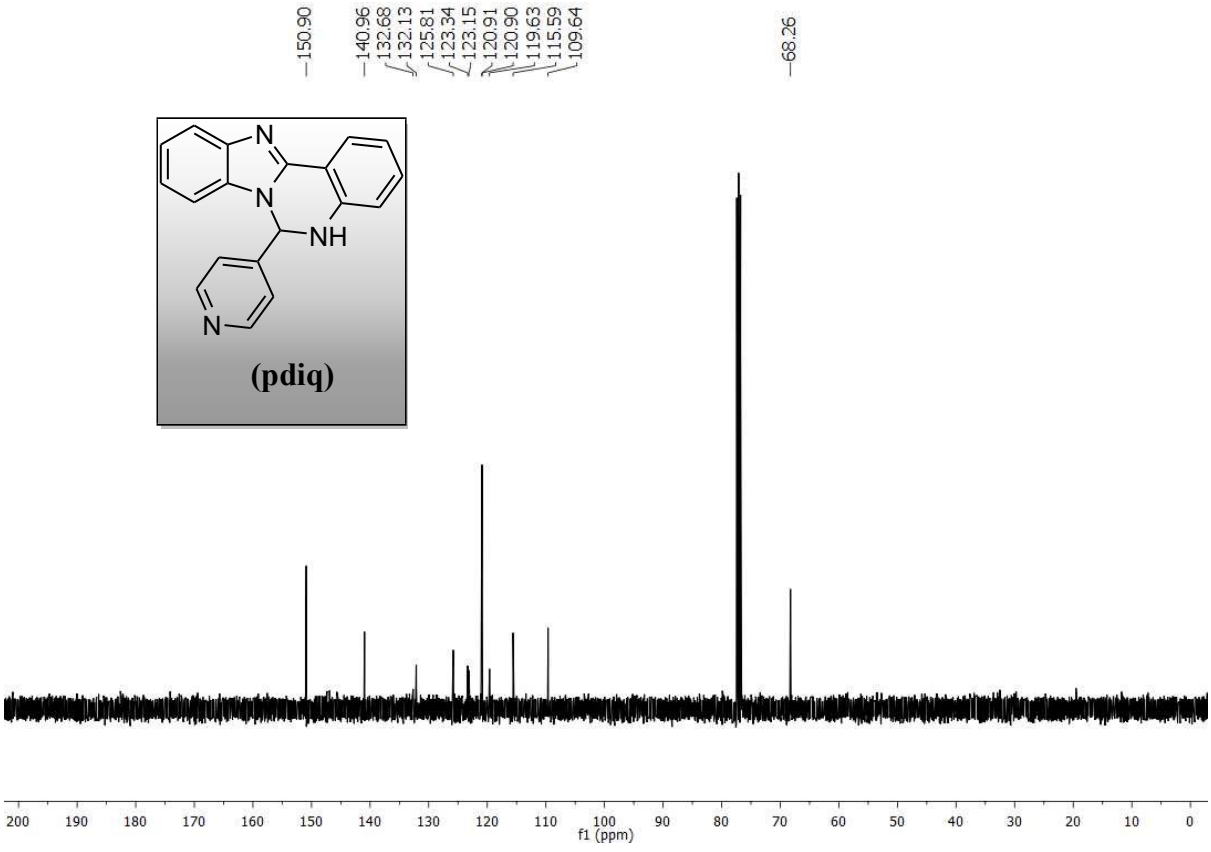

Fig. S3 ^{13}C-NMR spectrum of **pdiq**.

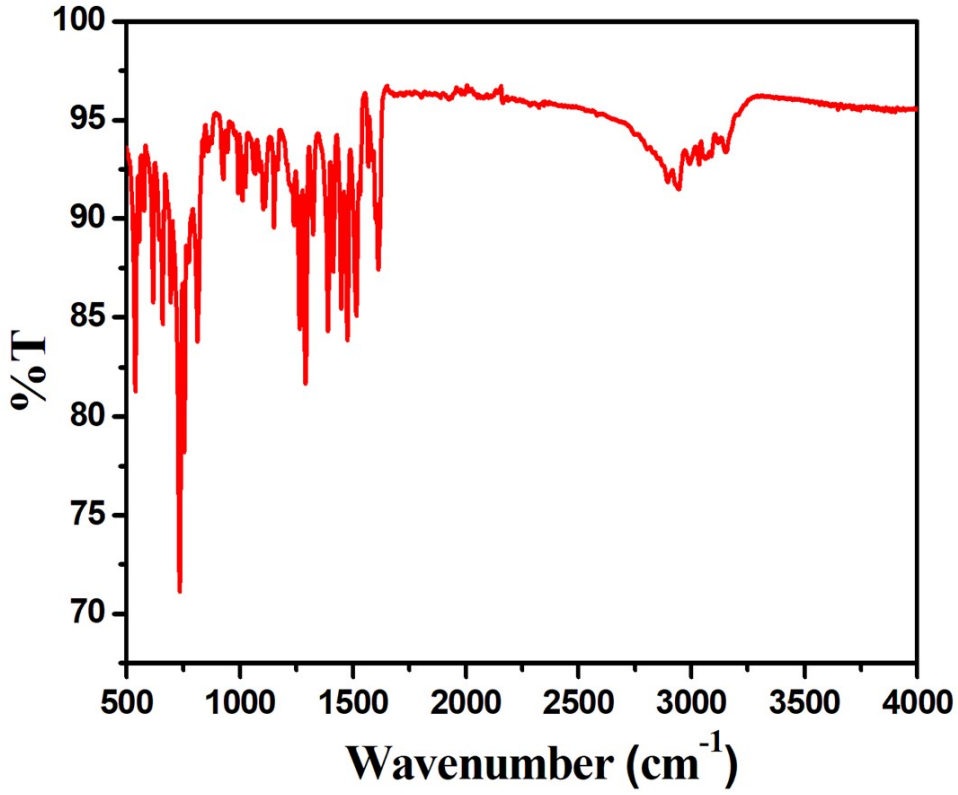

Fig. S4 IR spectrum of **pdiq**.

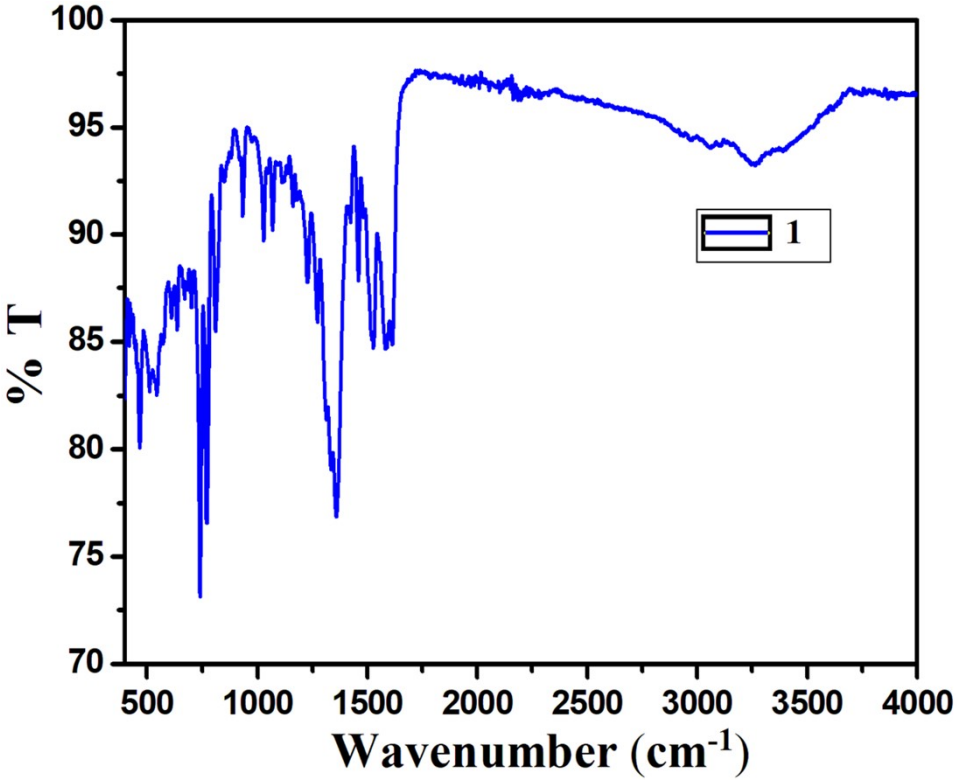

Fig. S5 IR spectrum of **1**.

Table S1. Crystal data and refinement parameters for **1**.

Formula	$C_{25}H_{16}N_4O_4SZn$
CCDC	2162910
Formula weight	533.87
Crystal system	Orthorhombic
space group	*'F d d d'*
a (Å)	11.4312(13)
b (Å)	31.433(4)
c (Å)	57.919(6)
α(deg)	90
β(deg)	90
γ (deg)	90
V (Å^3)	20811(4)
Z	32
D_{calcd}(g/cm^3)	1.363
μ(mm^{-1})	1.061
λ(Å)	0.71073
data[$I > 2\sigma(I)$]/params	4587/369
GOF on F^2	1.1344
final *R* indices[$I > 2\sigma(I)$][a,b]	$R1 = 0.0623$ $wR2 = 0.2169$

$^aR1 = \Sigma||F_o| \quad |F_c||/ \Sigma|F_o|$, $^bwR2 = [\Sigma w(F_o^2 \quad F_c^2)^2/\Sigma w(F_o^2)^2]^{1/2}$

Table S2. Selected bond lengths and bond angles in **1**.

Zn(1) - O(1)	2.010(7)	O(1)y - Zn(1) - N(3)y	114.1(3)
Zn(1) - O(2)	2.530(6)	O(3) - Zn(2) - O(3)s	81.67(18)
Zn(1) - N(3)	2.088(5)	O(3) - Zn(2) - N(4)w	152.1(2)
Zn(1) - O(1)y	2.010(7)	O(4) - Zn(2) - N(4)t	105.3(2)
Zn(1) - O(2)y	2.530(6)	O(3)s - Zn(2) - N(4)t	152.1(2)
Zn(1) - N(3)y	2.088(5)	O(4)s - Zn(2) - N(4)w	105.3(2)
Zn(2) - O(3)	2.555(6)	O(1) - Zn(1) - O(1)y	123.2(3)
Zn(2) - O(4)	2.006(8)	O(2) - Zn(1) - N(3)	168.9(2)
Zn(2) - O(3)s	2.555(6)	N(3) - Zn(1) - N(3)y	103.17(19)
Zn(2) - O(4)s	2.006(8)	O(2)y - Zn(1) - N(3)y	168.9(2)
Zn(2) - N(4)t	2.061(4)	O(3) - Zn(2) - O(4)s	95.3(2)
Zn(2) - N(4)w	2.061(4)	O(4) - Zn(2) - O(3)s	95.3(2)
O(1) - Zn(1) - O(2)	57.0(3)	O(4) - Zn(2) - N(4)w	97.9(2)
O(1) - Zn(1) - O(2)y	81.3(2)	O(3)s - Zn(2) - N(4)w	94.49(17)
O(2) - Zn(1) - O(1)y	81.3(2)	N(4)t - Zn(2) - N(4)w	101.02(17)
N(3) - Zn(1) - O(1)y	100.6(2)	Zn(2) - O(3) - C(25)	78.0(5)
O(1)y - Zn(1) - O(2)y	57.0(3)	Zn(1) - N(3) - C(3)	131.6(5)
O(3) - Zn(2) - O(4)	55.4(3)	Zn(1) - O(1) - C(20)	103.1(6)
O(3) - Zn(2) - N(4)t	94.49(17)	Zn(2) - O(4) - C(25)	104.4(6)
O(4) - Zn(2) - O(4)s	143.3(3)	Zn(1) - N(3) - C(9)	122.8(4)
O(3)s - Zn(2) - O(4)s	55.4(3)	Zn(1) - O(2) - C(20)	79.6(5)
O(4)s - Zn(2) - N(4)t	97.9(2)	C(18) - N(4) - Zn(2)g	118.7(3)
O(1) - Zn(1) - N(3)	114.1(3)	C(17) - N(4) - Zn(2)g	124.6(4)
O(1) - Zn(1) - N(3)y	100.6(2)		
O(2) - Zn(1) - O(2)y	86.10(19)		
N(3) - Zn(1) - O(2)y	85.82(19)		

Symmetry Code: g = -1/4+x, 1-y, -1/4+z; y = 3/4-x, 3/4-y, z; s = 7/4-x, y, 3/4-z; t = 3/2-x, 1-y, 1/2-z; w = 1/4+x, 1-y, 1/4+z.

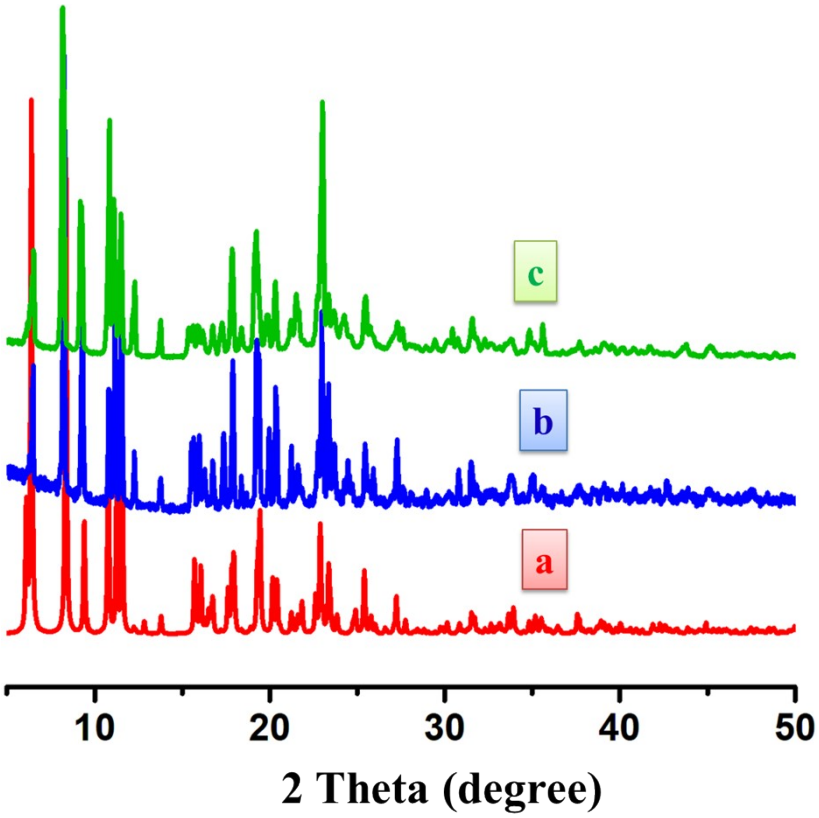

Fig. S6 PXRD patterns of a) simulated from the X-ray single structure of **1** (red), b) as-synthesized **1** (blue) and c) **1** after the prolonged immerged in lower pH solution (pH=4) (green).

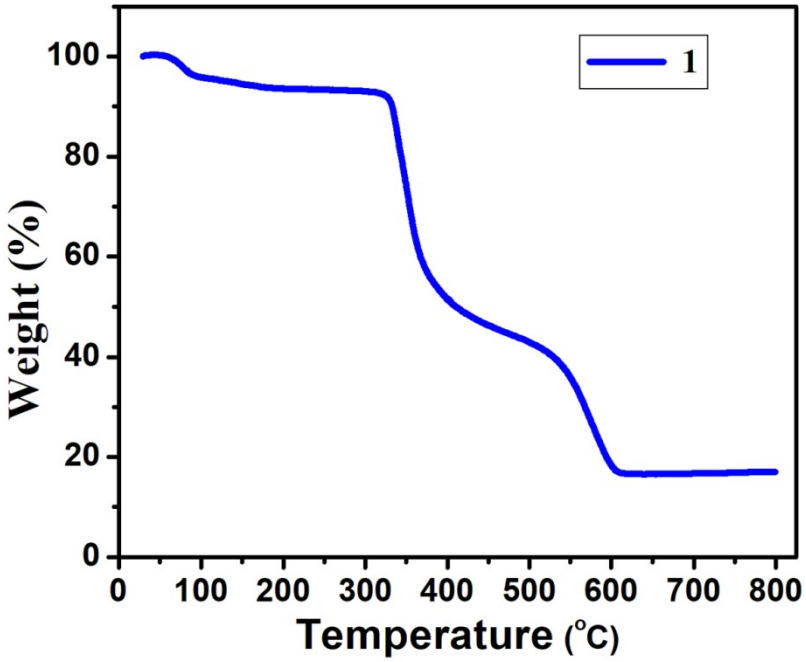

Fig. S7 TGA plot of **1**.

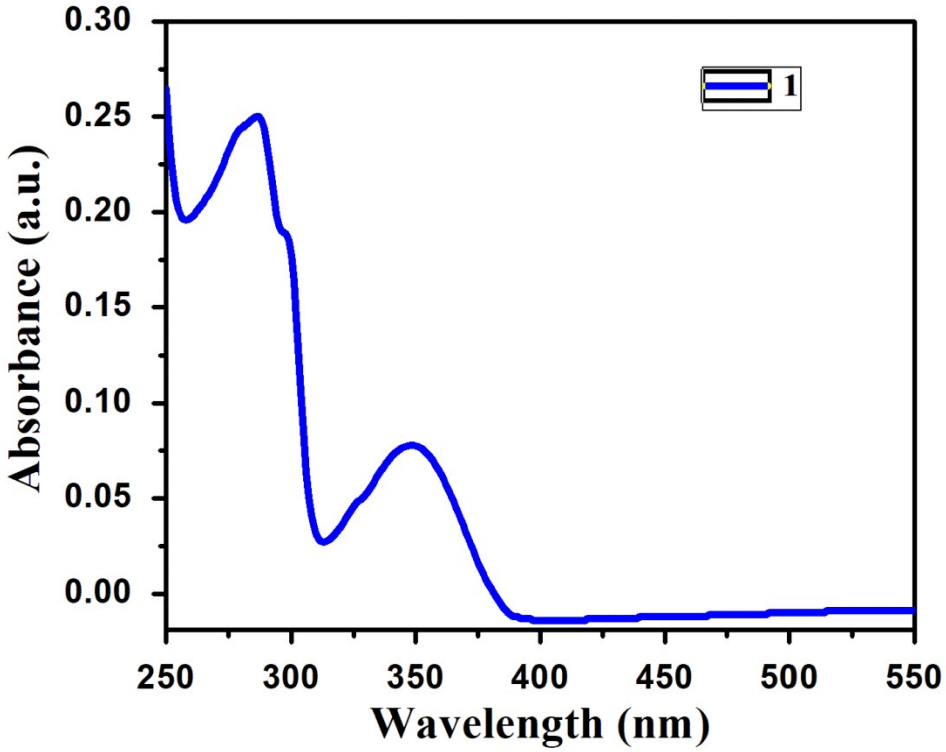

Fig. S8 UV-Visible spectrum of **1** in acetonitrile.

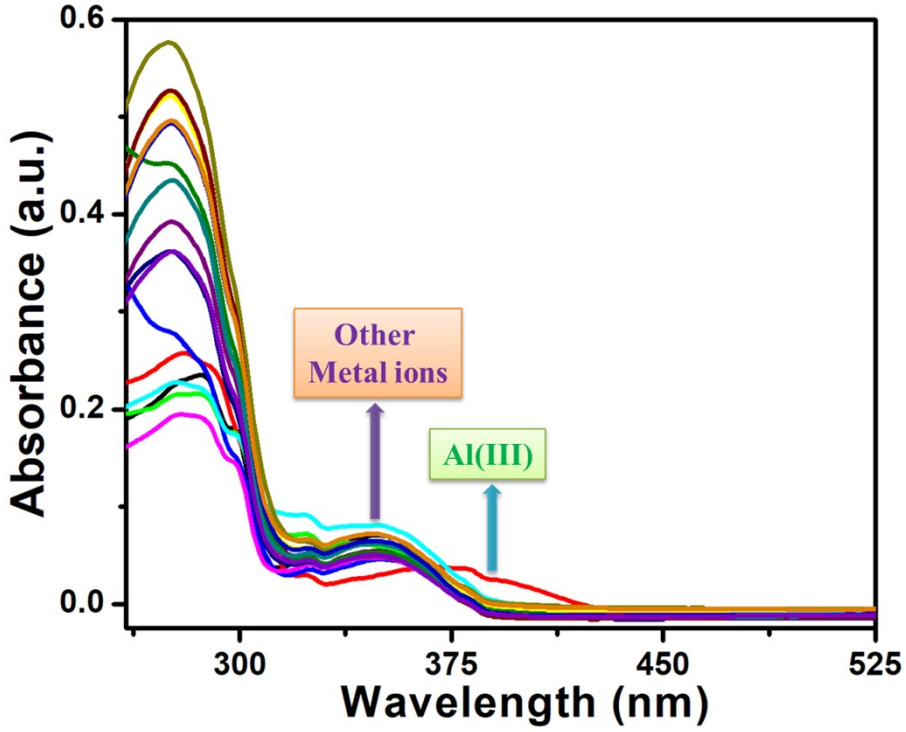

Fig. S9 Absorption spectra of **1** dispersed in CH_3CN in presence of different metal ions.

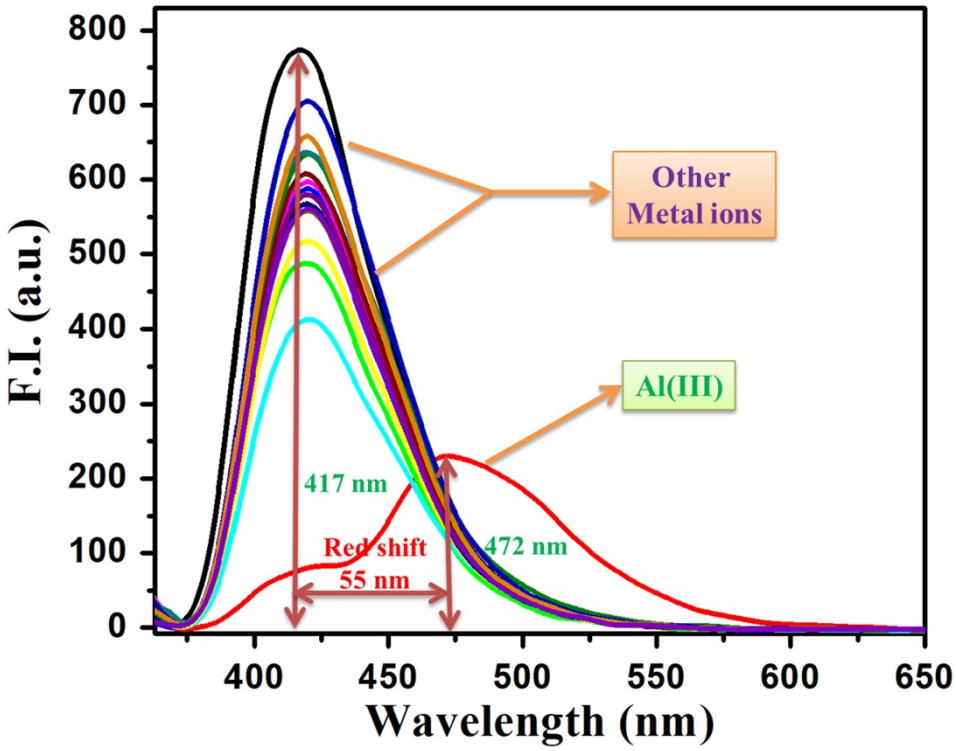

Fig. S10 Emission spectra of **1** dispersed in CH_3CN in presence of different metal ions.

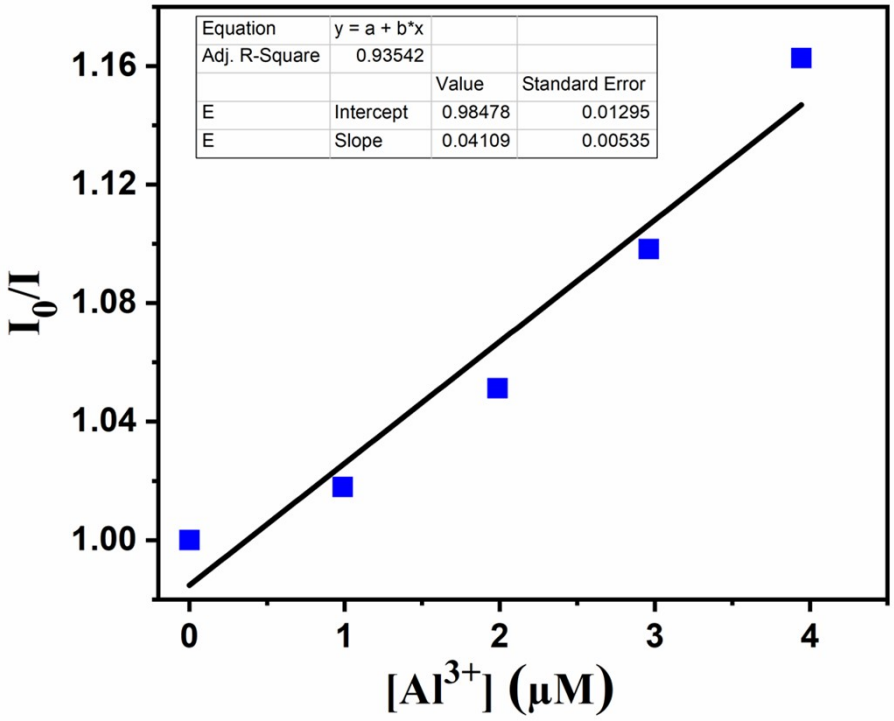

Fig. S11 Stern-Volmer plot of **1** at lower range of quencher [Al(III)] (in μM) concentration.

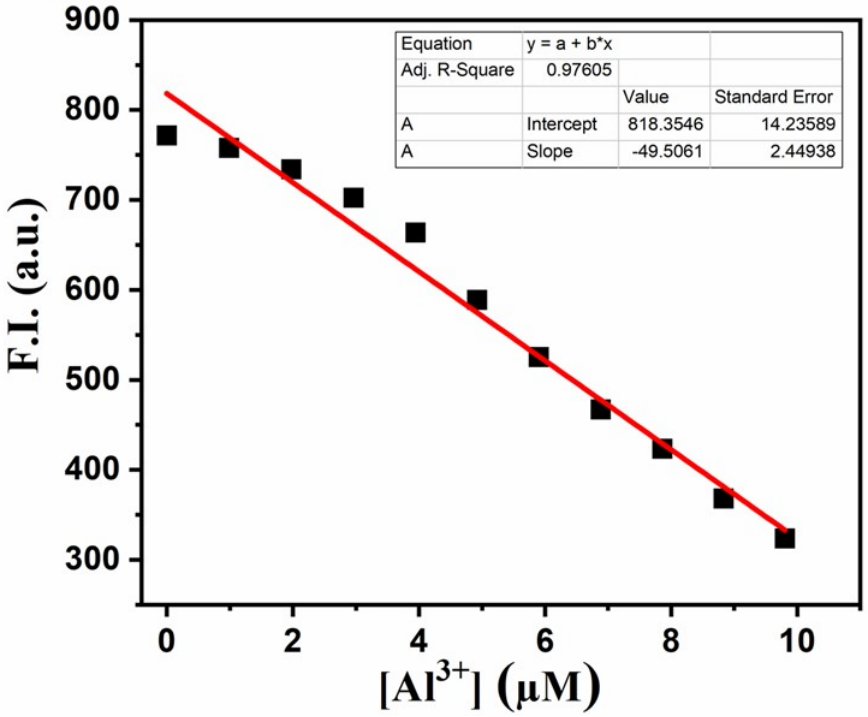

Fig. S12 The linear dynamic response of **1** for Al(III) and the determination of the limit of detection (LOD) of Al(III).

Detection limit calculation of 1 for Al(III):

The limit of detection (LOD) was calculated by using the equation: LOD = $3\sigma/K$, where 'σ' represents the standard deviation of blank titration of **1**. 'K' is the slope determined from the titration curve of **1** in presence of Al(III) at lower concentration. The plot of change in fluorescence intensity versus concentration of Al(III) revealed a linear curve (**Fig. S12**) with a slope (K) of 49.51 × 10^6 M^{-1} and correlation coefficient (R^2) of 0.976. The detection limit of **1** for Al(III) sensing was found to be 1.39 × 10^{-7} M, which is comparable with other reported MOF-based sensor materials.[1-6]

$$\text{Slope } (k) = 49.51 \times 10^6 \text{ M}^{-1}$$

$$\text{Standard Deviation } (\sigma) = 2.29$$

$$\text{Detection limit } (3\sigma/k) = 0.139 \ \mu\text{M}$$

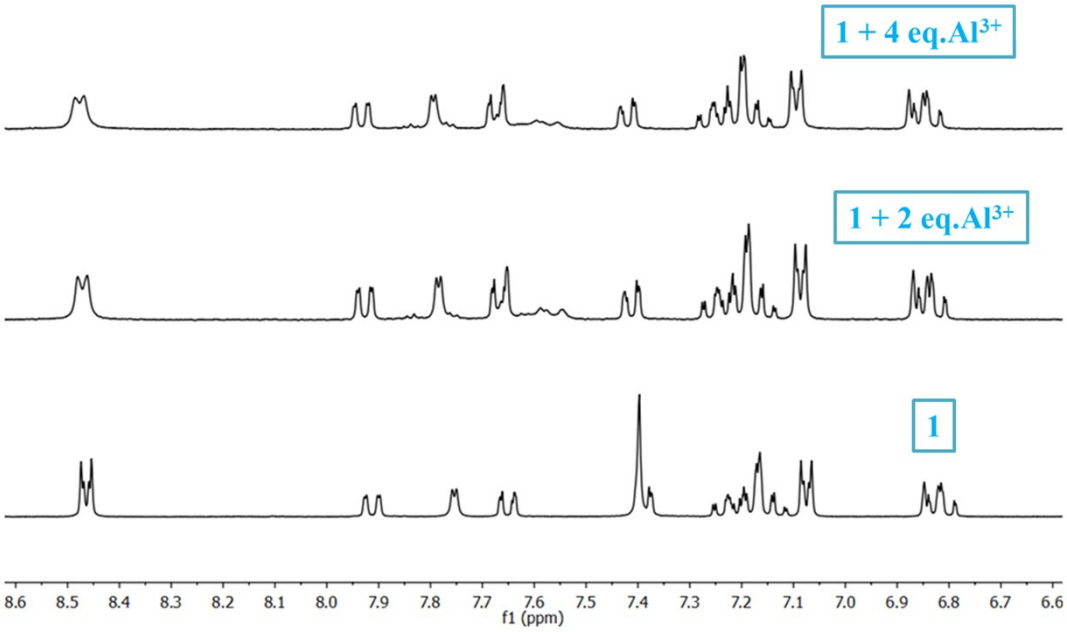

Fig. S13 ^{1}H-NMR titration between **1** and Al^{3+} in d^{6}-DMSO medium.

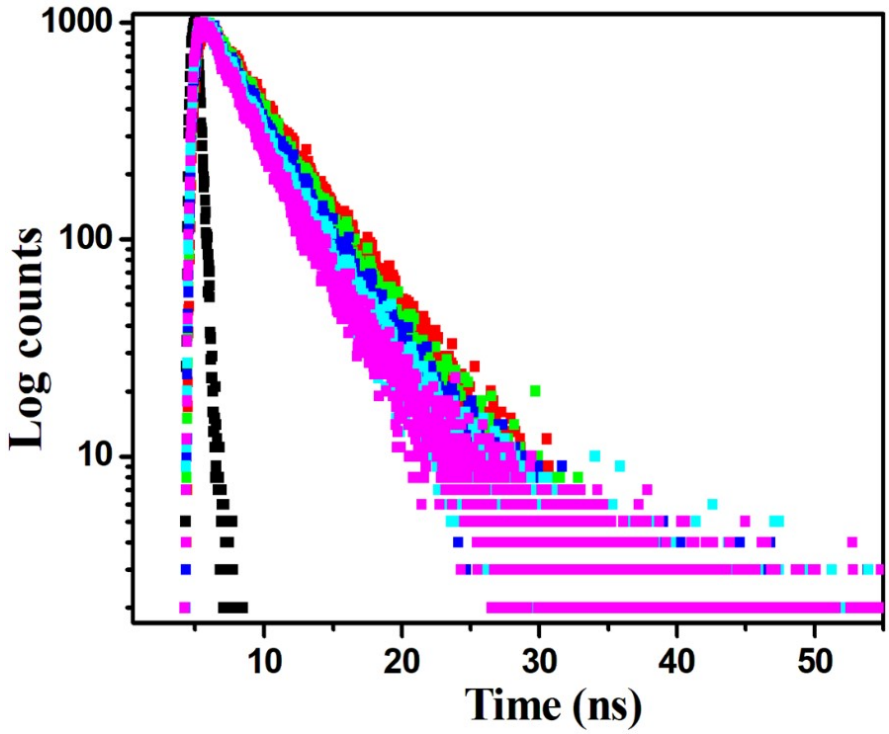

Fig. S14 Representative fluorescence decay spectra of **1** (10 μM) in the absence and presence of an increasing concentration of Al(III). Spectra 1-5 corresponds to the Al(III) concentration 0 μM (red square), 9.80 μM (green square), 19.42 μM (blue square), 28.85 μM (cyan square), 38.10 μM (magenta square), respectively.

Table S3. Fluorescence lifetime decay parameters of **1** (10 μM) with the gradual addition of Al(III).

Al(III) (μM)	τ (ns)	CHISQ
0	4.58	1.168835
9.80	4.21	1.17219
19.42	3.97	1.247764
28.85	3.69	1.215121
38.10	3.57	1.233064

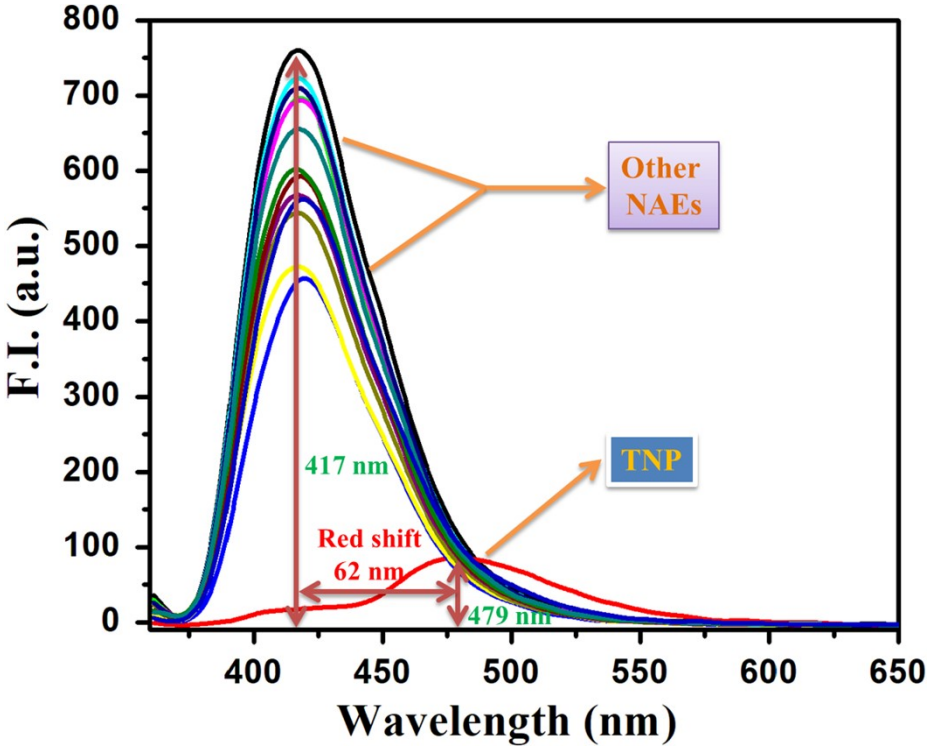

Fig. S15 Emission spectra of **1** dispersed in CH_3CN in presence of different Nitro Aromatic Explosives (NAEs).

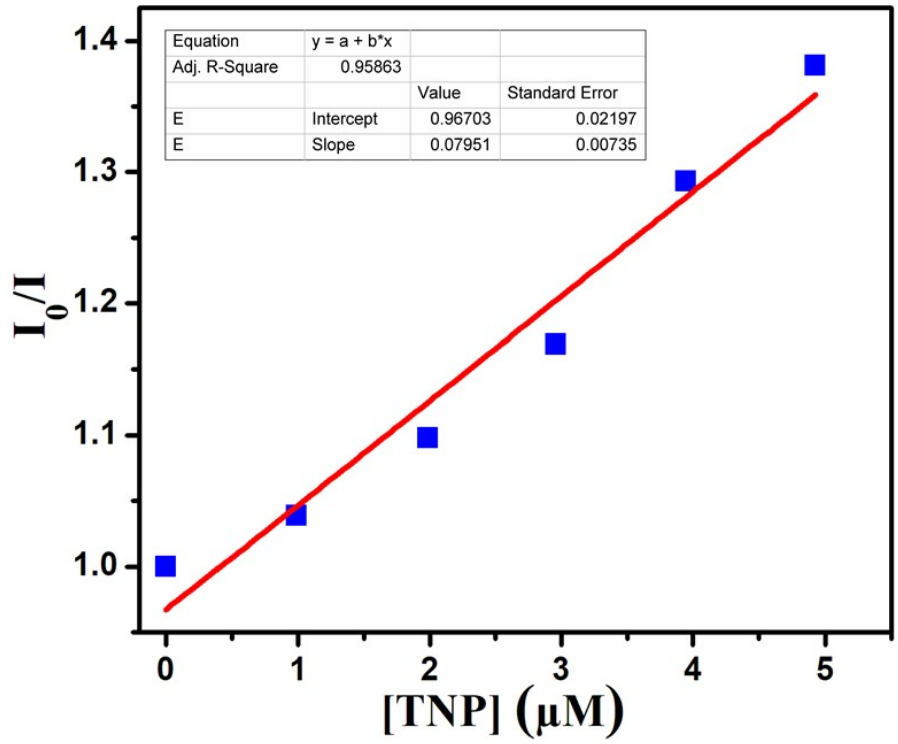

Fig. S16 Stern-Volmer plot of **1** at lower range of quencher [TNP] (in µM) concentration.

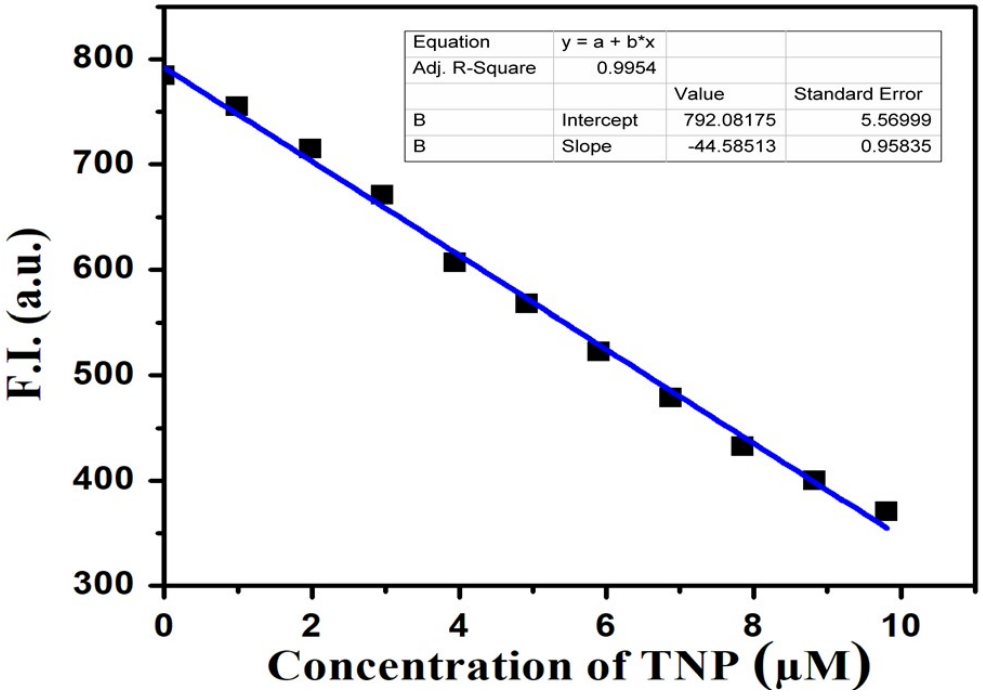

Fig. S17 The linear dynamic response of **1** for TNP and the determination of the limit of detection (LOD) of TNP.

Detection limit calculation of 1 for TNP

The limit of detection (LOD) was calculated by using the equation: LOD = $3\sigma/K$, where 'σ' represents the standard deviation of blank titration of **1**. 'K' is the slope determined from the titration curve of **1** in presence of TNP at lower concentration. The plot of change in fluorescence intensity versus concentration of TNP revealed a linear curve (**Fig. S17**) with a slope (K) of 44.59 × 10^6 M^{-1} and correlation coefficient (R^2) of 0.995. The detection limit of **1** for TNP sensing was found to be 1.54×10^{-7} M, which is comparable with other reported MOF-based sensor materials.[7-13]

Slope (k) = 44.59 × 10^6 M^{-1}

Standard Deviation (σ) = 2.29

Detection limit ($3\sigma/k$) = 0.154 μM

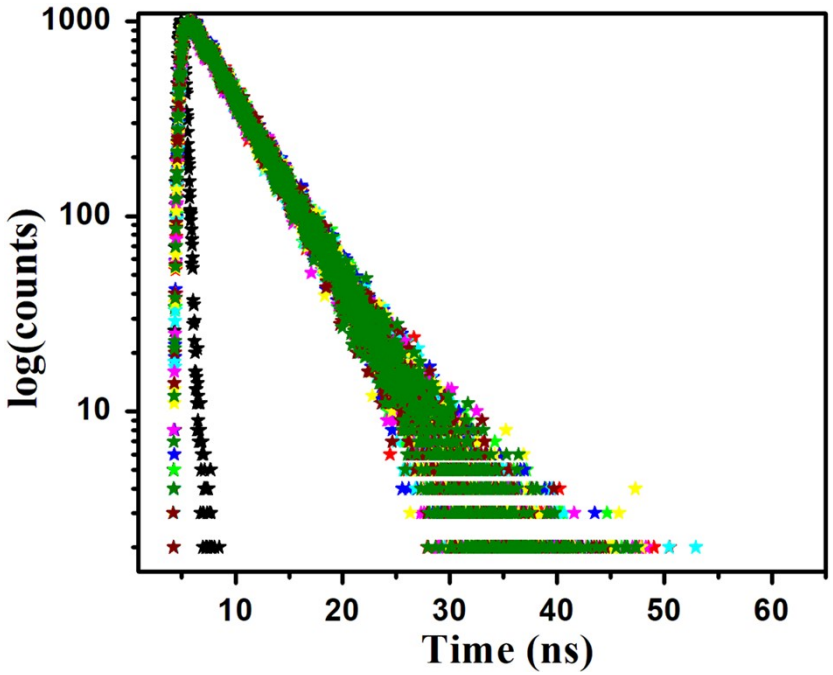

Fig. S18 Representative fluorescence decay spectra of **1** (10 μM) in the absence and presence of increasing concentration of TNP. Spectra 1-9 corresponds to the TNP concentration 0 µM (red star), 2.47 µM (green star), 4.93 µM (blue star), 7.37 µM (cyan star), 9.80 µM (magenta star), 14.63 µM (yellow star), 19.42 µM (wine star), 28.85 µM (navy star), 38.10 µM (olive star), respectively.

Table S4. Fluorescence lifetime decay parameters of **1** (10 μM) with gradual addition of TNP.

TNP (μM)	τ (ns)	CHISQ
0	4.67	1.245963
2.47	4.60	1.214508
4.93	4.57	1.237810
7.37	4.61	1.178241
9.80	4.57	1.231402
14.63	4.59	1.283751
19.42	4.58	1.187734
28.85	4.55	1.275290
38.10	4.55	1.275290

Table S5. HOMO and LUMO energies calculated for **1**.

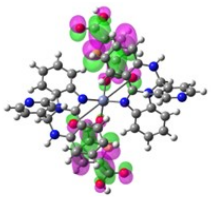	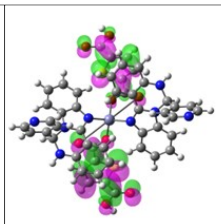	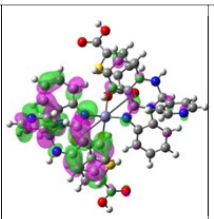	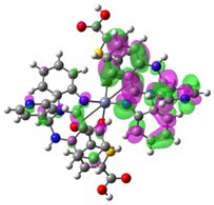	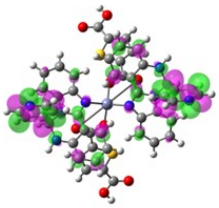
LUMO **E**=-2.14 eV **Zn** = 1% **Ligands** = 99%	**LUMO+ 1** **E**=-2.11 eV **Zn** = 0% **Ligands** = 100%	**LUMO+2** **E**=-1.95 eV **Zn** = 0% **Ligands** = 100%	**LUMO+3** **E**=-1.94 eV **Zn** = 0% **Ligands** = 100%	**LUMO+4** **E**=-1.58 eV **Zn** = 0% **Ligands** = 100%
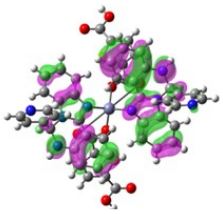	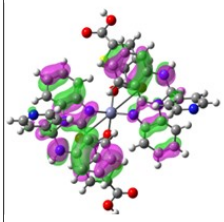	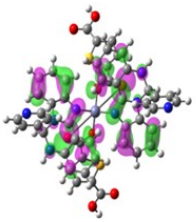	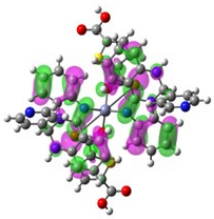	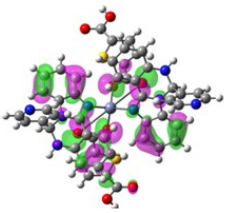
HOMO **E**=-5.99 eV **Zn** = 0% **Ligands** = 100%	**HOMO -1** **E**=-6.01 eV **Zn** = 0% **Ligands** = 100%	**HOMO -2** **E**=-6.53 eV **Zn** = 0% **Ligands** = 100%	**HOMO -3** **E**=-6.55 eV **Zn** = 0% **Ligands** = 100%	**HOMO -4** **E**=-6.66 eV **Zn** = 0% **Ligands** = 100%

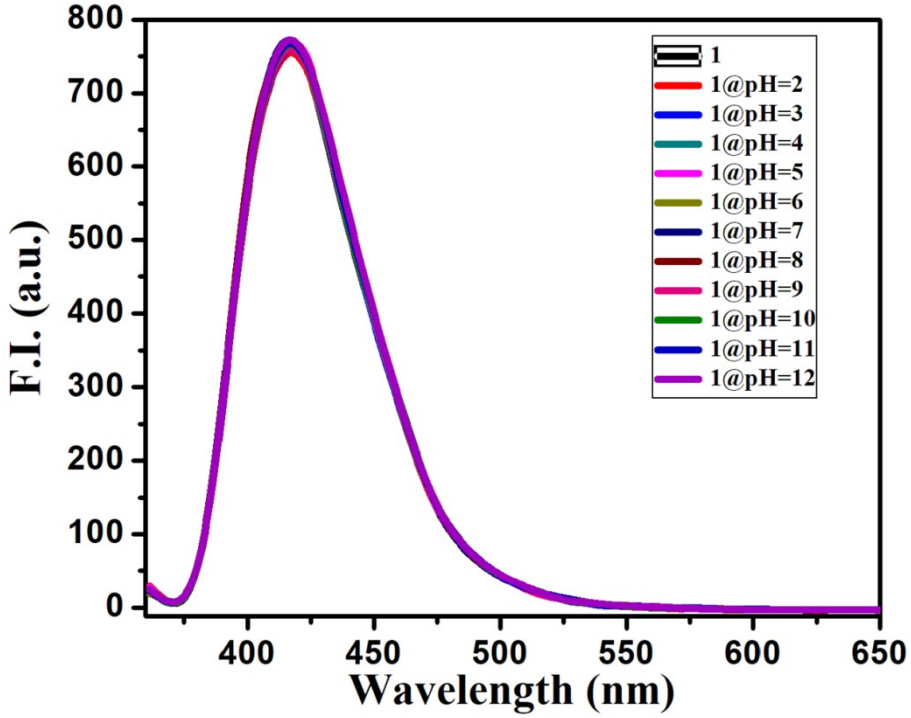

Fig. S19 Emission spectra of **1** in presence of different pH solutions.

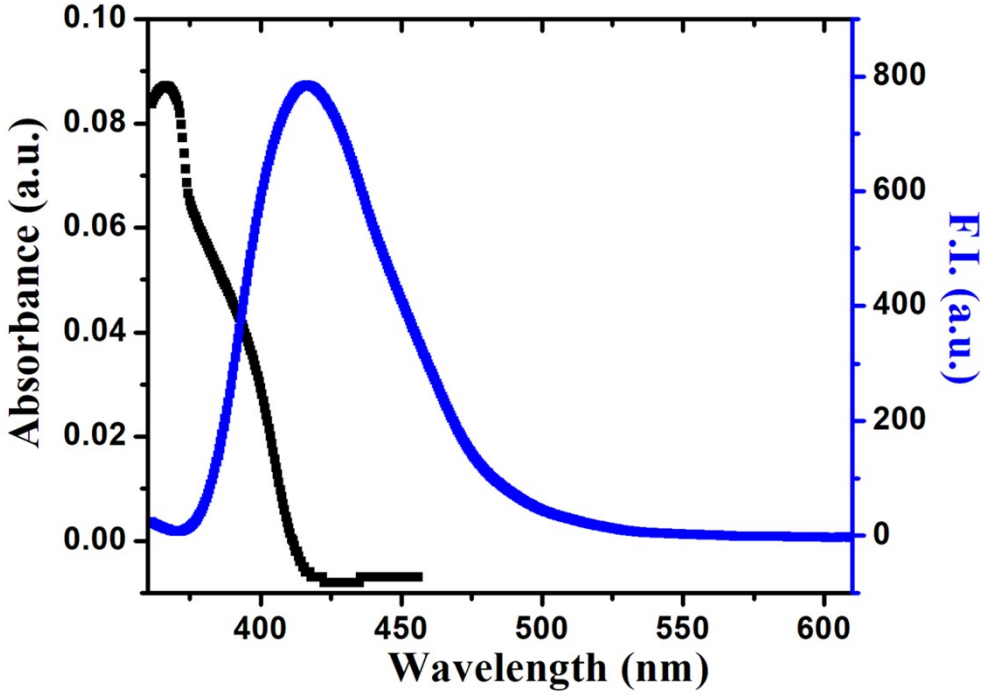

Fig. S20 Overlapping of absorption spectra of TNP with emission spectra of **1**.

.

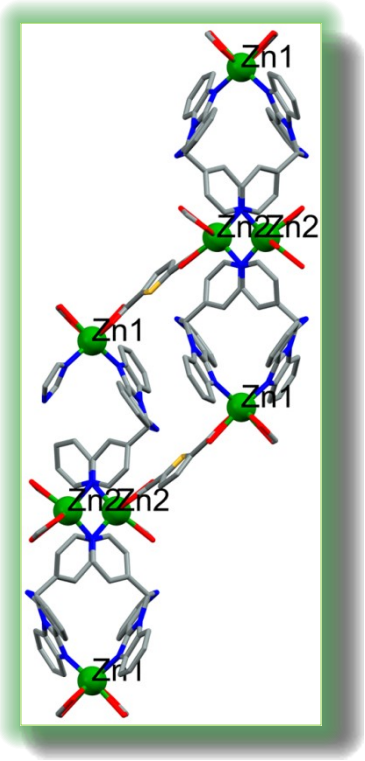

Fig. S21 One dimensional **(**1D) ribbon like network from a portion of molecular assembly of **1**.

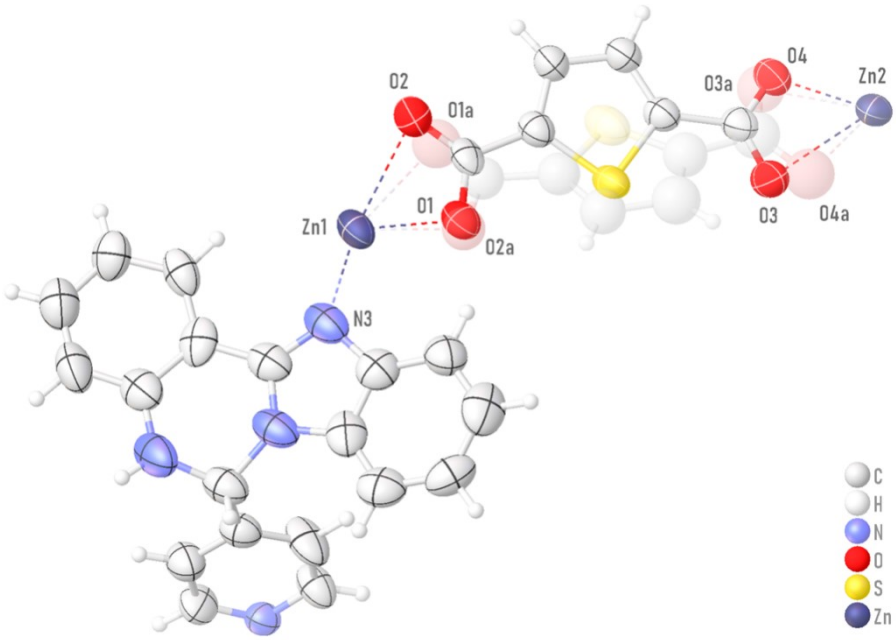

Fig. S22 The ORTEP diagram of **1** showing disorder of 2,5-tda ligand.

(Thanks to the Reviewer for sharing the structures)

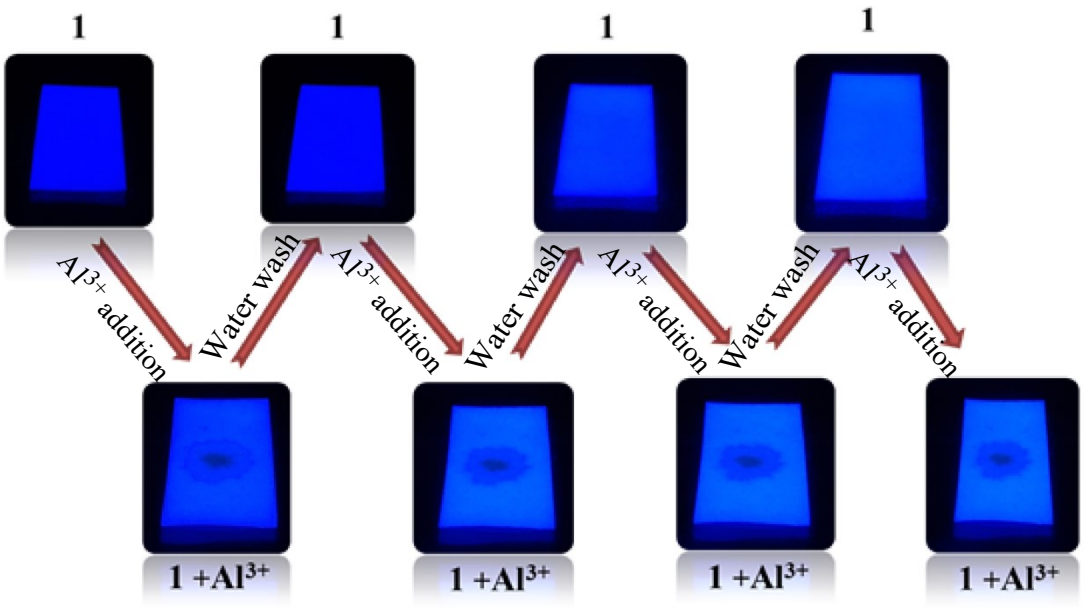

Fig. S23 Paper strip experiment for recyclability of Zn-MOF (**1**) towards Al^{3+} sensing.

Optical Characterization

The optical band gap (Eg) was calculated using Tauc's equation (Equation S1).[14]

$$(\alpha h\nu) = A(h\nu - E_g)^n \quad \text{(S1)}$$

where α, E_g, h and ν stands for absorption coefficient, band gap, Planck's constant and frequency of light. The exponent 'n' is the electron transition processes dependent constant. 'A' is a constant which is considered as 1 for ideal case. To calculate the direct optical bandgap the value of the exponent 'n' in the above equation has been considered as n = ½.[14] By extrapolating the linear region of the plot $(\alpha h\nu)^2$ *vs.* $h\nu$ to α = 0 absorption, the values of optical

direct band gap (E_g) have been calculated as 3.33 eV for synthesized compound (**1**).

Device Fabrication

In this study, multiple metal-semiconductor (MS) junction devices were fabricated in ITO/synthesized **1**/Al sandwich structure to perform the electrical study. In this regard, well dispersion of the synthesized complexes were made in N,N-dimethyl formamide (DMF) by mixing and sonicated the right proportion (25 mg/ml) of the complex in a vial. This freshly prepared stable dispersion of the compound was deposited on the top of the ITO coated glass substrate by spun firstly at 600 rpm for 5 min and thereafter at 900 rpm for another 5 min with the help of SCU 2700 spin coating unit. Afterward, the as-deposited thin film was dried in a vacuum oven at 80 °C for several minutes to evaporate the solvent part fully. Here we used aluminium as metal electrode, which was deposited using Vacuum Coating Unit on the active layer of the devices by maintaining the effective area as 7.065×10^{-2} cm^{-2} with shadow mask. Using Sourcemeter made by Keithley (model no: 2401), the current-voltage (*I-V*) characteristics of the devices was measured to analyze the electrical properties. All the device fabrication and measurements were carried out at room temperature and under ambient conditions.

Electrical Characterization

The $I-V$ characteristic of **TFD 1** was further analyzed by thermionic emission theory. Cheung's method was also been employed to extract important diode parameters.[14] In this regard, the obtained $I-V$ curve was analyzed quantitatively by considering the following standard equations:[14,15]

$$I = I_0 exp\left(\frac{qV}{\eta KT}\right)\left[1-exp\left(\frac{-qV}{\eta KT}\right)\right] \quad \text{(S2)}$$

$$I_0 = AA^* T^2 exp\left(\frac{-q\emptyset_B}{KT}\right) \quad \text{(S3)}$$

where, I_0, k, T, V, A, η and A^* stands for saturation current, electronic charge, Boltzmann constant, temperature in Kelvin, forward bias voltage, effective diode area, ideality factor and effective Richardson constant, respectively. The effective diode area has been estimated as 7.065×10^{-2} cm^2 and the effective Richardson constant has been considered as 32 $AK^{-2}\,cm^{-2}$ for all the devices.

The series resistance, ideality factor and barrier potential height was also determined by using equations S4 to S6, which was extracted from Cheung's idea,[16,17]

$$\frac{dV}{d(lnI)} = \left(\frac{\eta KT}{q}\right) + IR_S \quad \text{(S4)}$$

$$H(I) = V-\left(\frac{\eta KT}{q}\right)\ln\left(\frac{I}{AA^* T^2}\right) \quad \text{(S5)}$$

$$H(I) = IR_S + \eta\emptyset_B \quad \text{(S6)}$$

From the saturated values of capacitance at the higher frequency regime (**Fig. S24**) the dielectric permittivity of the complex was calculated using following equation:[18]

$$\varepsilon_r = \frac{1}{\in_0}.\frac{C.D}{A} \quad \text{(S7)}$$

where, C is the capacitance (at saturation), D is the thickness of the film which has been considered as ~1 μm and A is the effective area. Using the above

formula, the relative dielectric constant of the material has been estimated as 3.66×10^{-1} for **TFD 1**.

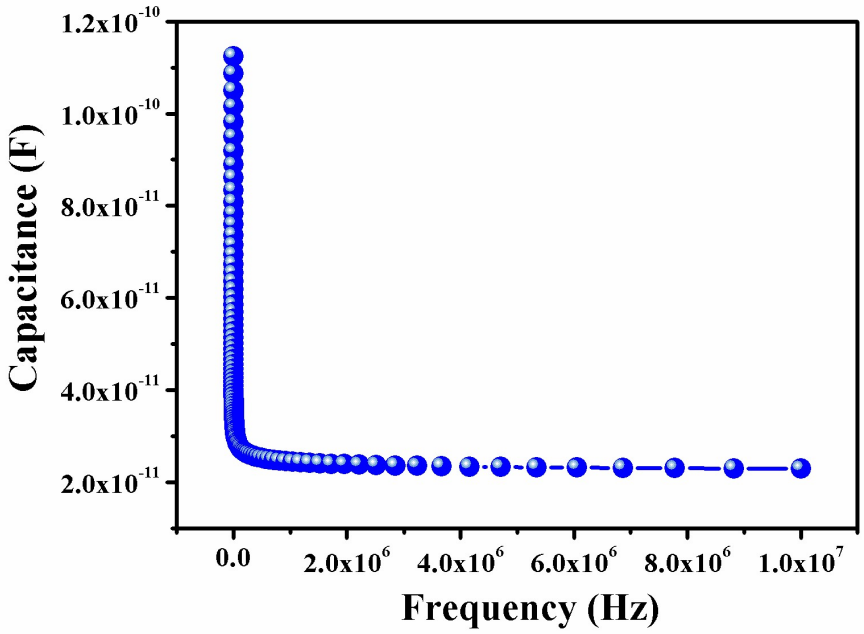

Fig. S24 Capacitance vs. Frequency graph of **TFD 1**.

References

1 Y. E. Yu, Y. Wang, H. Yan, J. Lu, H. Liu, Y. Li, S. Wang, D. Li, J. Dou, L. Yang and Z. Zhou, *Inorg. Chem.*, 2020, **59**, 3828-3837.

2 X. Zhang, X. Luo, N. Zhang, J. Wu and Y. Q. Huang, *Inorg. Chem. Front.*, 2017, **4**, 1888-1894.

3 W. X. Li, J. H. Gu, H. X. Li, M. Dai, D. J. Young, H. Y. Li and J. P. Lang, *Inorg. Chem.*, 2018, **57**, 13453-13460.

4 Y. Qiao, Z. Li, M. H. Yu, Z. Chang and X. H. Bu, *CrystEngComm.*, 2021, **23**, 8087-8092.

5 S. T. Wang, X. Zheng, S. H. Zhang, G. Li and Y. Xiao, *CrystEngComm.*, 2021, **23**, 4059-4068.

6 S. Chand, G. Verma, A. Pal, S. C. Pal, S. Ma and M. C. Das, *Chem. -Eur. J.*, 2021, **27**, 11804-11810.

7 B. Dutta, A. Hazra, A. Dey, C. Sinha, P. P. Ray, P. Banerjee and M. H. Mir, *Cryst. Growth Des.*, 2020, **20**, 765-776.

8 G. Bairy, A. Dey, B. Dutta, P. P. Ray and C. Sinha, *Cryst. Growth Des.*, 2022, **22**, 3138-3147.

9 K. S. Asha, K. Bhattacharyya and S. Mandal, *J. Mater. Chem. C*, 2014, **2**, 10073-10081.

10 S. S. Nagarkar, A. V. Desai and S. K. Ghosh, *Chem. Commun.*, 2014, **50**, 8915-8918.

11 S. S. Nagarkar, B. Joarder, A. K. Chaudhari, S. Mukherjee and S. K. Ghosh, *Angew. Chem. Int. Ed.*, 2013, **52**, 2881-2885.

12 X. Z. Song, S. Y. Song, S. N. Zhao, Z. M. Hao, M. Zhu, X. Meng, L. L. Wu and H. Zhang, *J. Adv. Funct. Mater.*, 2014, **24**, 4034-4041.

13 A. Buragohain, M. Yousufuddin, M. Sarma and S. Biswas, *Cryst. Growth Des.*, 2016, **16**, 842-851.

14 A. Dey, S. Middya, R. Jana, M. Das, J. Datta, A. Layek and P. P. Ray, *J. Mater. Sci. Mater. Electron.*, 2016, **27**, 6325-6335.

15 E. H. Rhoderick, Metal Semiconductors Contacts, Oxford University Press, Oxford. 1978.

16 S. K. Cheung and N. W. Cheung, *Appl. Phys. Lett.*, 1986, **49**, 85-87.

17 A. Dey, A. Layek, A. Roychowdhury, M. Das, J. Datta, S. Middya, D. Das and P. P. Ray, *RSC Adv.*, 2015, **5**, 36560-36567.

18 A. Dey and S. K. Ray, *Int. J. Adv. Sci. Eng.*, 2020, **6**, S2-1-6.